

## LUMINESCENCE AND STRUCTURAL PROPERTIES ON $\text{Sm}^{3+}$ DOPED KBr SINGLE CRYSTALS

S.Bangaru<sup>1\*</sup>, D.Roobanguru<sup>2</sup>

<sup>1\*</sup>Associate Professor of Physics, Arignar Anna Govt. Arts College, Namakkal.

<sup>2</sup>Ph. D Research Scholar in Physics, Arignar Anna Govt. Arts College, Namakkal

---

**Abstract:-** Single crystals of  $\text{Sm}^{3+}$  doped KBr were grown by vertical Bridgmann Stockbarger technique. The grown crystal were subjected to the characterization such as Optical absorption, Photoluminescence (PL), Thermoluminescence (TL), and TL emission, studies. The Optical absorption, TL studies on KBr:  $\text{Sm}^{3+}$  crystals irradiated with  $\gamma$ -rays is reported. The shoulder around 348nm is due to formation of V-band and bell shaped band at 611nm are noticed because of F-band formation in Optical Absorption spectrum. Under the excitation of 405nm light, the emission spectra were governed by the characteristic reddish-orange luminescence primarily originated due to transition from the excited  $^4\text{G}_{5/2}$  to the  $^6\text{H}_{7/2}$  lower level noticed at 603nm. Thermoluminescence (TL) glow peak reveals two clearly visible distinct peaks at temperature around 464K and 491K. The calculated kinetic parameters show that both peaks follow the second order kinetics.

---

**Key words:** KBr,  $\text{Sm}^{3+}$ , PL, TL

### 1. Introduction

Alkali halides are simplest ionic solids to study the optical properties of rare earth metals by doping into them. The luminescence properties are strongly influenced by impurities doped into samples and largely depends on the host materials. There is permanent interest in investigating spectroscopic properties of rare earth ions incorporated into different inorganic host lattice from the view point of basic research and various applications of such luminescent materials. Potassium halide is an efficient host lattice for the luminescence of various rare earth ( $\text{Ce}^{3+}$ ,  $\text{Tb}^{3+}$ ) ions [1, 2]. Samarium is an active ion for different inorganic host lattice and act as a powerful emitting centre due to its energy level structure and high luminescence efficiency [3]. It is widely used as an excellent activator to produce orange (or) reddish orange emission from different inorganic host lattices because of its  $^4\text{G}_{5/2} \rightarrow ^6\text{H}_J$  ( $J=5/2, 7/2, 9/2, 11/2$ ) transitions[4,5]. The large ionic radius of potassium ions permits incorporation of a large number of cationic impurities. The sites of dopants determined by their ionic radii. The radii of  $\text{Sm}^{3+}$  are 0.958. Most of the work has been done in samarium doped materials as powder and glasses [6,7,8]. Not much work could be traced to samarium in the crystalline lattice. Considering the wide range of samarium in different kind of matrices, an attempt has been made to study Photoluminescence (PL), Thermoluminescence (TL) and structural properties of KBr:  $\text{Sm}^{3+}$  crystal grown by Bridgmann Stockbarger technique.

### 2. Experimental

Single crystals of Samarium doped KBr (99.99% purity) were grown using Bridgmann Stockbarger technique. Samarium was added in the form of Samarium fluoride (Aldrich 99.99% purity). The crystal grown with three different impurity concentrations 1%, 3% and 5% by weight. The results due to three concentrations were similar except high luminescence yield for crystals with a high concentration. Hence only the results pertaining to Samarium concentration of 5% by weight are presented and discussed. All the measurements were performed at room temperature. Optical absorption spectrum were recorded using Perkin Elmer Lambda 35 UV-Vis spectrophotometer in the wavelength range 190- 1100nm. PL spectra were recorded at room temperature using Perkin Elmer LS 55 fluorescence spectrophotometer from 200nm to 900nm width spectral with of 5nm. TL glow curve were recorded using PC based TL analyser (integrated type TL1009I) when the crystal irradiated with  $\gamma$  -ray dose of 5 Gy at a heating rate of 5°C/sec. TL emission were recorded in Perkin Elmer LS 55 with excitation slit being closed.

### 3. Optical Absorption

The optical absorption spectrum of  $\text{Sm}^{3+}$  doped KBr crystal recorded in the wavelength range 190nm-990nm before and after  $\gamma$ -ray irradiation for 1-hour is shown in Fig.1 curve (a) and (b) respectively. The assignment of bands in the UV-Vis region is not easy because of the overlap of different  $^{2s+1}L_J$  levels. Before irradiation, the broad absorption band observed around 226nm and 230nm which attributed to the exciton absorption of the host matrix. The shoulder observed around 257nm and 417nm in Fig.1 curve (a) assigned to excitation of electron states from ground levels of samarium ions. So it confirms that samarium ions absorb UV light in this wavelength region. After irradiation, the band observed at 202nm and 306nm are shifted to lower wavelength and broadened due to accumulation of more electrons in the trapping centre. The shoulder around 348nm is due to formation of V-band and bell shaped band at 611nm are noticed because of F-band formation. This shows the formation of formation of electron trap centre and hole trap centre near the conduction band and valence band respectively within the forbidden gap of host matrix. The formation of F-band in RbI doped with  $\text{Sm}^{3+}$  crystals is at 770nm for 6 hr of  $\gamma$ -ray irradiation [9].

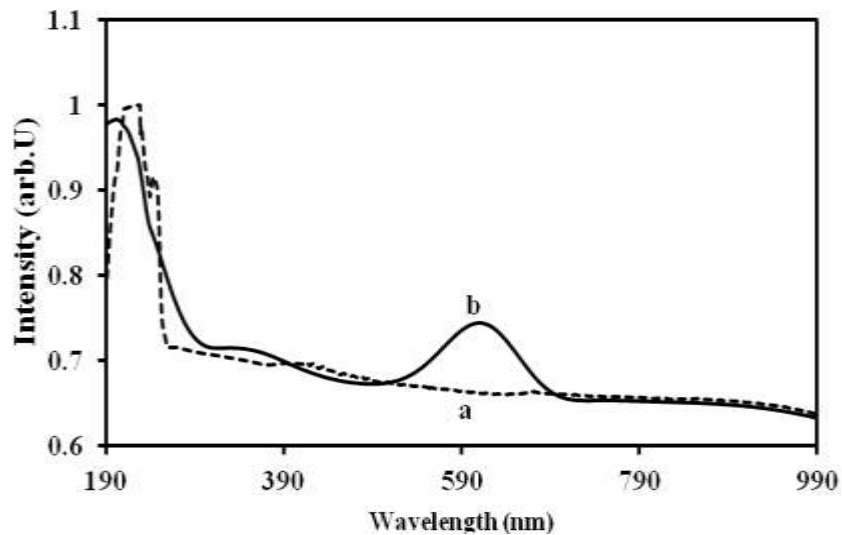


**Fig.1 Optical Absorption spectrum curve (a) before irradiation, curve (b) after irradiation  $\gamma$ -ray irradiation for 1-hour of KBr :  $\text{Sm}^{3+}$  single crystals**

The absorption bands identified are due to transition of  $^6\text{H}_{5/2}$  ground state to various excited energy states. The absorption bands are more intense and broad in the UV region due to effective shielding of 4f electrons by the filled 5s and 5p shells [10]. From the spectrum, it has been inferred that unirradiated KBr:  $\text{Sm}^{3+}$  crystals have sufficient transmission nearly in the entire visible region. The absorption co-efficient is high at lower wavelength and the transparency in the visible part of the spectrum from 450nm suggesting their suitability for luminescent materials. The bandgap energy of unirradiated KBr :  $\text{Sm}^{3+}$  crystals with the maximum wavelength absorption (226nm) is calculated by using the simple conversion equation  $E=hc/\lambda_{\text{max}}$  [11]. The calculated bandgap is 4.6eV. Pure KBr has the bandgap value of 7.6eV. This value is reduced by the incorporation of samarium as impurity into KBr host.

### 4. Photoluminescence (PL)

Fig.2 curve (a) and Fig.2 curve (b) represents the PL excitation and PL spectra of KBr :  $\text{Sm}^{3+}$  single crystals respectively. The PL excitation spectrum shows a narrow band covering the spectral range 380nm to 430nm under 600nm monitoring, indicative of the strong absorption of UV light. The excitation band centered at 405nm are assigned to the  $^6\text{H}_{5/2} \rightarrow ^4\text{F}_{7/2}$  transition of samarium ion. PL spectrum of KBr :  $\text{Sm}^{3+}$  crystal monitored at the  $^6\text{H}_{5/2} \rightarrow ^4\text{F}_{7/2}$  transition wavelength (405nm). When the samarium ions were excited to the  $^4\text{F}_{7/2}$  level, then relax to the  $^4\text{G}_{5/2}$  level by non-radiative relaxation and then come to the ground level  $^4\text{H}_{7/2}$  by radiative emission. This radiative emission gives the characteristic emission of  $\text{Sm}^{3+}$  emission [12]. Under the excitation of 405nm light, the emission spectrum were governed by the characteristic reddish-orange luminescence primarily originated due to transition from the excited  $^4\text{G}_{5/2}$  to the  $^6\text{H}_{7/2}$  lower level noticed at 603nm. The emission wavelength of grown crystal at longer wavelength side indicates that it

is used for illuminating devices. Similar emission transitions have been observed in  $\text{Sm}^{3+}$  ion doped glasses [13,14]. The excitation spectrum of  $\text{Sm}^{3+}$  doped KBr compared with the optical absorption spectrum which is shown in table.1 and found that the transition due to  $\text{Sm}^{3+}$  ions are similar around 400nm.

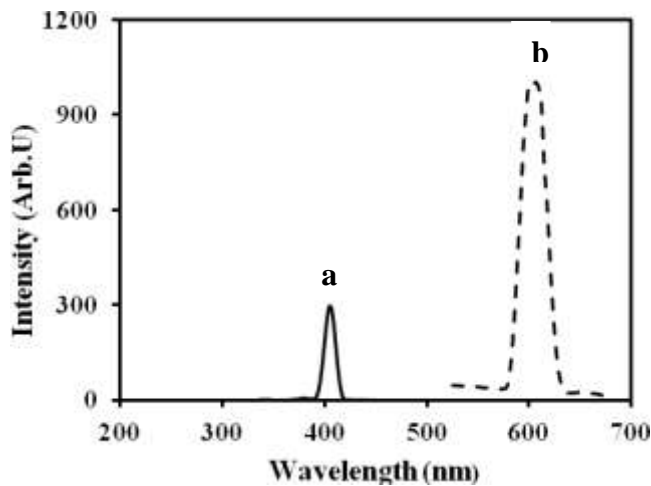


Fig.2 Photoluminescence of KBr :  $\text{Sm}^{3+}$  crystals (a) Excitation spectrum for emission at 600nm (b) Emission spectrum for excitation at 405nm

Table.1 Comparison of wavelength in Optical absorption, Photoluminescence and Deconvoluted TL emission of KBr:  $\text{Sm}^{3+}$  crystals

Optical absorption		Photoluminescence		Deconvoluted TL Emission
Before irradiation	After irradiation	Excitation bands	Emission bands	Emission band at 491K
Wavelength (nm)	Wavelength (nm)	Wavelength (nm)	Wavelength (nm)	Wavelength (nm)
226	202	405	603	590
230	306	$(^6\text{H}_{5/2} \rightarrow ^4\text{F}_{7/2})$	$(^4\text{G}_{5/2} \rightarrow ^6\text{H}_{7/2})$	630
257(shoulder)	348(V-band)			
417 (shoulder)	611(F-band)			

### 5. Thermoluminescence (TL) glow curve

TL technique is a useful tool for revealing the nature of trapping centres produced in crystal upon irradiation using X-rays, UV-light and  $\gamma$ -rays[15,16]. Thermoluminescence glow curve were recorded soon after  $\gamma$ -ray irradiation for 1hour of the sample to avoid the possibility of the error. The electrons trapped upon irradiation can be released from the traps due to subsequent heating and this process results in TL signal. TL spectrum will be composite when several traps are emptied under heating due to the sum of single TL peaks [17-19]. The TL glow curve is roughly deconvoluted by means of using software ‘Origin 5.0’. Fig.3 shows the deconvoluted TL glow curve of KBr :  $\text{Sm}^{3+}$  crystals after  $\gamma$ -ray irradiation for 1hour. TL is observed upto 560°K at a heating rate of 120°C/min. The deconvoluted glow curve locating two peak centered at 464K and 491K which demonstrate that the introduction of  $\text{Sm}^{3+}$  into the KBr matrix has produced the two trap centres within the KBr host. This is the suitable behaviour for dosimetric applications. But the TL intensity of this sample is small compared with the standard TLD material and therefore does not have any direct application in dosimetry. The characteristics of dosimeters used in TL process are related to kinetic parameters and the evaluated parameters quantitatively describe the trapping emitting centres. The study of kinetic parameters such as activation energy (E) and frequency factor(s) provides information related to defect centres responsible for TL in the material[20,21]. There are various methods for evaluating kinetic parameters from TL glow curve. In this work, the

parameters can be calculated by means of using Chen’s peak shape method. This method is a popularly used technique to determine the kinetic parameters of the glow peak. The TL glow curve can be divided into two glow peaks at 464K and 491K. The kinetic parameters mainly based on the temperature  $T_1$ ,  $T_m$  and  $T_2$ , where  $T_m$  is the glow peak temperature and  $T_1$ ,  $T_2$  are the temperature at half intensity on low temperature and high temperature side of the glow peak respectively. The following shape parameters were evaluated for the determination of kinetic parameters:  $\omega = T_2 - T_1$  (total half intensity width),  $\delta = T_2 - T_m$  (high temperature half width) and  $\tau = T_m - T_1$  (low temperature half width).

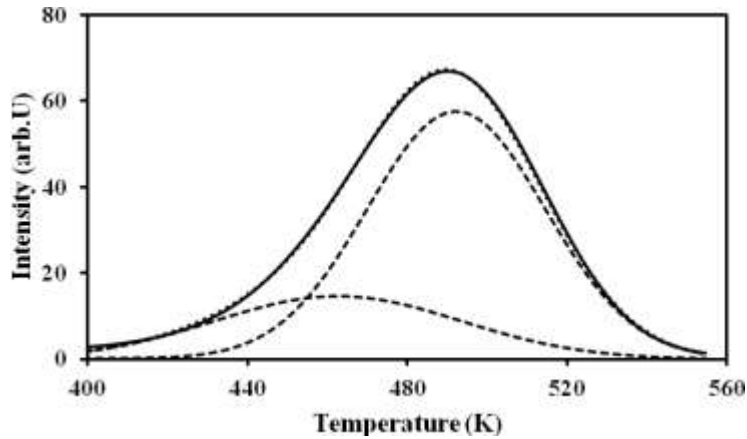


**Fig.3 Deconvoluted Thermoluminescence glow curve of KBr :  $Sm^{3+}$  crystals after  $\gamma$ -ray irradiation for 1-hour**

The kinetic order can be determined from the symmetry factor ( $\mu_g$ ) of glow peak ( $\mu_g = \delta/\omega$ ) and depends on the shape of the glow peak. The value of  $\mu_g$  for first and second order kinetics is 0.42 and 0.52 respectively. The calculated kinetic parameters were tabulated in table.2. For both glow peaks, the geometric factor is around 0.5 and indicates that the crystal obeys second order kinetics. The activation energy (E) and frequency factor (s) can be calculated by the equation reported in earlier work [16,22]. The activation energy E (eV) and Frequency factor s ( $sec^{-1}$ ) for 464K peak are calculated as 1.804 and 2.43 ; for 491K peak these values are estimated as 1.160 and 2.62. The activation energy of two traps differ slightly. Therefore it evidenced that there is formation of some deep and shallow traps. The high temperature glow peak related with deep trap and the low temperature glow peak related with shallower trap[23]. The frequency factor values are also slightly different. This may be due to the competition among various traps might be giving various escaping and retrapping probabilities which resulted in different frequency factors. The traps may be either electron or hole trap or both. The concentration of charge carrier ( $n_0$ ) can be calculated by means of equation reported in earlier work [24]. This value is estimated as 1.67 and 0.58 for 464K and 491K respectively. This has appreciable different values. It shows that the more number of charge carriers are trapped at deep trap compared with shallow trap.

**Table.2 Calculated Kinetic Parameters of TL glow curve of KBr : $Sm^{3+}$  Crystal**

Glow Peak Temperature $T_g$ (K)	Intensity (arb.U)	Geometric factor $\mu_g = \delta/\omega$	Activation Energy E $\times 10^{-19}$ (eV)	Frequency factor s $\times 10^{-02}$ ( $S^{-1}$ )	Concentration of charge carriers $n_0$ ( $Cm^3$ ) <sup>-1</sup>	Order of kinetics
491	57	0.54	1.804	2.43	1.67	II
464	14	0.51	1.160	2.62	0.58	II

## 6. Thermoluminescence emission

Fig.4 curve (a) and curve (b) shows the TL emission spectrum of KBr :  $Sm^{3+}$  crystals at 464K and 491K respectively. TL emission spectra recorded for different rare earth (RE) dopants in alkali halide confirmed that in all case the TL emission

characteristic of  $RE^{3+}$  and it is also matching with  $RE^{3+}$  emission observed in respective PL spectra. This result show a correlation for PL and TL emission in RE doped KBr crystal and in both process main emission occur from  $RE^{3+}$ . Fig.4 curve (a) exhibit emission band at 592nm and curve (b) shows emission at 580nm. The emission peak related with 491K glow peak was roughly deconvoluted using Software 'Origin 5.0'. The emission recorded for 491K glow peak is high intense due to trapping of more charge carriers at deep traps whereas emission recorded for 464 K glow peak is less intense because small number of carriers trapped at shallow traps. So we chose 491K glow peak for deconvolution. The deconvoluted emission spectrum were shown in fig.5. It gives two well distinguished peaks centered at 590nm and 630nm. This two emission bands in TL emission spectrum confirms the participation of samarium ions in the TL process. The presence of these emissions indicates the capture of an electron by  $Sm^{4+}$  ions possibly formed upon irradiation. This capture leaves a  $Sm^{3+}$  ion in an excited state, which on relaxation, yields 590nm and 630nm emission. In RbI :  $Sm^{3+}$ , Manimozhi et al.[25] reported emissions at 590nm, 650nm, 720nm and 740nm. Comparing these results with KBr:  $Sm^{3+}$ , it is observed that TL emission contain only the emission due  $Sm^{3+}$  ions. TL emission spectrum is attributed to the recombination of thermally released F-electrons with samarium ions and of hole centres. On comparing TL emission and PL spectrum (table.1), the emission band observed at 603nm in PL and 590nm in TL emission are similar. So the emission occur only due to the participation of samarium ions.

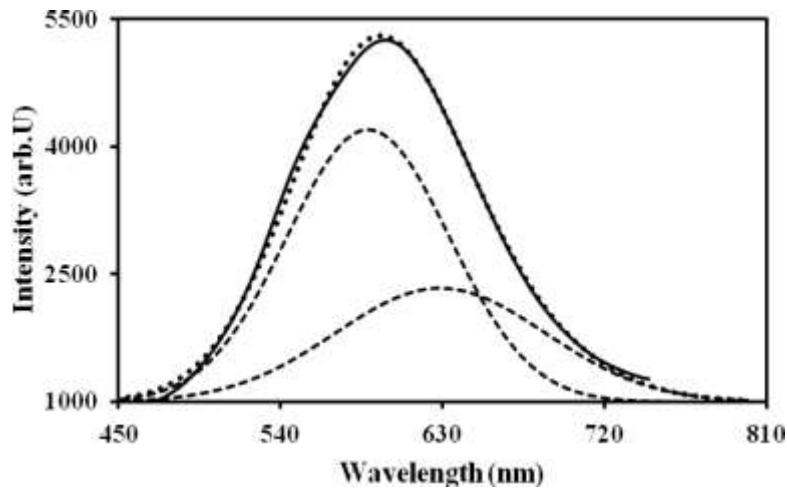


**Fig.5 Deconvoluted TL Emission KBr :  $Sm^{3+}$  crystals at 491K**

## 7. Conclusion

The shoulder around 348nm is due to formation of V-band and bell shaped band at 611nm are noticed because of F-band formation after  $\gamma$ -ray irradiation. Under the excitation of 403 light, the emission spectra were governed by the characteristic reddish-orange luminescence primarily originated due to transition from the excited  ${}^4G_{5/2}$  to the  ${}^6H_{7/2}$  lower level noticed at 603nm. The emission wavelength of grown crystal at longer wavelength side indicates that it is used for illuminating devices. Thermoluminescence (TL) glow peak reveals two clearly visible distinct peaks at temperature around 464K and 491K. The calculated kinetic parameters show that both peaks follow the second order kinetics.

## Acknowledgements

Authors sincerely thank and gratefully acknowledge UGC-DAE Consortium for Scientific Research, IGCAR, Kalpakkam for providing experimental facilities for this work.

## REFERENCES

1. S.Bangaru, G.Muralidharan, Enhanced Luminescent Properties and Optical Absorption of  $\gamma$ -Irradiated Ki:  $Ce^{3+}$ ,  $Tb^{3+}$  Crystals, Journal of Luminescence, vol.129, pp.24-29, (2009).
2. S.Bangaru, Photoluminescence and EPR studies on gamma irradiated  $Ce^{3+}$  doped potassium halide single crystals, Physica B, vol.406, pp.159-164, (2011).

3. M.B.Reddy, C.N.Raju, S.Sailaja, B.V.Rao, B.S.Reddy, Sol–Gel Synthesis, Structural and Optical Properties of Rare Earth Ions ( $\text{Sm}^{3+}$  Or  $\text{Dy}^{3+}$ ) Activated  $\text{Ca}_3\text{Ga}_2\text{Si}_3\text{O}_{12}$  Powder Phosphors, *Journal of Luminescence*, vol.131, pp.2503-2508, (2011).
4. P.Solarz, G.Dominiak, R.Lisiecki, W.Ryba-Romanowski, E.Beregi, I.Foldvari, K.Lengyel, Spectroscopic properties of  $\text{Sm}^{3+}$  impurity in  $\text{YAl}_3(\text{BO}_3)_4$  single crystal, *Optical Materials*. vol.32, pp.1446-1450, (2010).
5. A.Thulasiramudhu, S.Buddhudu, Optical Characterization of  $\text{Sm}^{3+}$  and  $\text{Dy}^{3+}:\text{ZnO-PbO-B}_2\text{O}_3$  Glasses, *Spectrochimica Acta Part A*. vol.67 (2007) pp. 802-807.
6. K.Swapna, S.K. Mahamuda, A.Srinivasa Rao, S.Shakya, T.Sasikala, D.Haranath, G.Vijaya Prakash, Optical studies of  $\text{Sm}^{3+}$  ions doped Zinc Alumino Bismuth Borate glasses, *Spectrochimica Acta Part A: Molecular and Biomolecular Spectroscopy*. vol.125, pp.53-60, (2014).
7. A.Agarwal, I.Pal, S.Sanghi, M.P.Aggarwal, Judd–Ofelt parameters and radiative properties of  $\text{Sm}^{3+}$  ions doped zinc bismuth borate glasses, *Optical Materials*, vol.32, pp.339-344, (2009).
8. Z.Wang, P.Li, Z.Yang, Q.Guo, A Novel Red Phosphor  $\text{BaZn}_2(\text{PO}_4)_2:\text{Sm}^{3+}, \text{R}^+$  ( $\text{R}=\text{Li}, \text{Na}, \text{K}$ ), *Journal of Luminescence*. vol.132, pp.1944-1948, (2012).
9. P.K.Manimozhi, G.Muralidharan, Luminescence and Laser Raman studies on gamma-irradiated  $\text{RbI}:\text{Sm}^{3+}$  crystals, *Physica Status Solidi (b)*. vol.244, pp.3730-3738, (2007).
10. Y.K.Sharma, S.S.L.Surana, R.K.Singh, Spectroscopic investigations and luminescence spectra of  $\text{Sm}^{3+}$  doped soda lime silicate glasses, *Journal of Rare Earths*, vol. 27, pp. 773-780, (2009).
11. B.Want, M.D.Shah, Growth and Characterization of Terbium Fumarate Heptahydrate Single Crystal, *Journal of Crystal Growth*, vol.389, pp.39-46, (2014).
12. Y.I.Jeon, L.Krishna Bharat, J.S.Yu, White-light emission of  $\text{Ca}_2\text{La}_8(\text{GeO}_4)_6\text{O}_2:\text{Tb}^{3+}/\text{Sm}^{3+}$  nanocrystalline phosphors for solid-state lighting applications, *Journal of Luminescence*. vol.166, pp. 93-100, (2015).
13. P.R.Biju, G.A.Kumar, N.V.Unnikrishnan, Spectroscopic studies of  $\text{Sm}^{3+}$  doped phosphate glasses, *Bulletin of Material Science*, vol. 21, pp.415-419, (1998).
14. C.K.Jayasankar, P.Babu, Optical Properties Of  $\text{Sm}^{3+}$  Ions In Lithium Borate And Lithium Fluoroborate Glasses, *Journal of Alloys and Compounds*, vol.307, pp.82-95, (2000).
15. S.Basun, G.F.Imbusch, D.Jia, W.M.Yen, The Analysis of Thermoluminescence Glow Curves, *Journal of Luminescence*. vol.104, pp.283-294, (2003).
16. S.W.S.Mckeever, Thermoluminescence of solids, Cambridge University Press, Cambridge, New York, New Rochelle, Melbourne, Sydney, 1985.
17. D.Jia, W.M.Yen, Trapping Mechanism Associated with Electron Delocalization and Tunneling of  $\text{CaAl}_2\text{O}_4:\text{Ce}^{3+}$ , A Persistent Phosphor, *Journal of Electrochemical Society*, vol.150, pp.H61-H65, (2003).
18. D.Jia, W.M.Yen, Enhanced  $\text{V}_K^{3+}$  center afterglow in  $\text{MgAl}_2\text{O}_4$  by doping with  $\text{Ce}^{3+}$  *Journal of Luminescence*, vol.101, pp.115-121, (2003).
19. Y.Liu, B.Lei, C.Shi, Luminescent Properties of a White Afterglow Phosphor  $\text{CdSiO}_3:\text{Dy}^{3+}$ , *Chemistry of Materials*. vol.17, pp. 2108-2113, (2005).
20. S.J.Dhoble, S.V.Moharil, T.K.Gundu Rao, Correlated ESR, PL and TL studies on  $\text{K}_3\text{Na}(\text{SO}_4)_2:\text{Eu}$  thermoluminescence dosimetry phosphor, *Journal of Luminescence*. vol.93, pp.43-49, (2001).
21. S.J.Dhoble, S.V.Moharil, T.K.Gundu Rao, Correlated ESR, PL and TL studies on  $\text{Sr}_5(\text{PO}_4)_3\text{Cl}:\text{Eu}$  thermoluminescence dosimetry phosphor, *Journal of Luminescence*, vol.126, pp.383-386, (2007).
22. R.Chen, On the Calculation of Activation Energies and Frequency Factors from Glow Curves, *Journal of Applied Physics*, vol.40, pp.570-585, (1969).
23. S.P.Lochar, A.Pandey, P.D.Sahare, R.S.Chauhan, N.Salah, N.R.Ranjan, Nanocrystalline  $\text{MgB}_4\text{O}_7:\text{Dy}$  for high dose measurement of gamma radiation *Physica Status Solidi (a)*. vol. 204 (2007) pp.2416-2425.
24. Z.H.Ju, S.H.Zhang, X.P.Gao, X.L.Tang, W.S.Liu, Reddish Orange Long Afterglow Phosphor  $\text{Ca}_2\text{SnO}_4:\text{Sm}^{3+}$  Prepared by Sol–Gel Method, *Journal of Alloys and Compounds*, vol.509, pp.8082-8087, (2011).
25. P.K.Manimozhi, G.Muralidharan, Luminescence and laser Raman studies on gamma-irradiated  $\text{RbI}:\text{Sm}^{3+}$  crystals, *Physica Status Solidi (b)*, vol.244, pp.3730-3738, (2007).